Jet and Missing E_T Reconstruction and Signatures at ATLAS and CMS

K. Terashi [a] (For the ATLAS and CMS Collaborations)

[a]ICEPP, University of Tokyo, 7-3-1 Hongo, Bunkyo-ku, Tokyo 113-0033, Japan

Jet and missing transverse energy reconstruction and calibration strategies and their expected performance in the ATLAS and CMS experiments at the LHC are presented. Studies of high transverse momentum signatures of jets aimed at the search for new phenomena such as boosted top quark *mono*-jets expected in various beyond the standard model scenarios are also discussed.

ATL-PHYS-PROC-2009-137
28 November 2009

1. INTRODUCTION

A precise measurement of jets and missing transverse energy ($\not\!\!E_T$) is a powerful tool for many physics analyses at hadron colliders. Determination of the jet energy scale with an accuracy of 1 % (aimed in both experiments) is desired, e.g, for precision measurement of the top quark mass and reconstruction of the edge of kinematic distributions to determine the SUSY mass scale. However, jets, representing quarks and gluons observed as a collimated spray of final state particles, are not uniquely defined even theoretically and the ambiguity in jet energy measurement is further amplified by the smearing due to detector resolution and threshold effects. All the experimental ambiguities in conjunction with various detector and beam related backgrounds also lead to a mis-reconstructed $\not\!\!E_T$. Theoretically motivated reconstruction algorithms and flexible data-driven calibration strategies are needed to overcome these problems.

In this letter, reconstruction and calibration procedure for jets and $\not\!\!E_T$ in ATLAS and CMS experiments at the LHC are presented with an emphasis on jet calibration where a factorized data-driven calibration approach has been devised in both experiments. The $\not\!\!E_T$ reconstruction usually starts with calorimeter signal and the calibration is applied after $\not\!\!E_T$ reconstruction, depending on different physics objects in the event. A 'particle-flow' algorithm where jets and $\not\!\!E_T$ are reconstructed from all identified particles in an event has been studied in CMS. [1] Details of the algorithm and its performance in physics events are discussed in a later section. Finally, a signature of high transverse momentum jets is explored from the viewpoint of new phenomena search beyond the standard model including high-p_T jets with a sub-jet structure, expected in boosted top quark production from heavy resonances decaying to a top-antitop quark pair.

2. CALORIMETERS

The main detector component for jet and $\not\!\!E_T$ reconstruction is the calorimeter system. A wide pseudorapidity coverage of about $-5.0 < \eta < 5.0$ by both ATLAS [2] and CMS [3] calorimeters ensures full geometric acceptance for the measurement of particle transverse energies in an event. The technologies chosen by both experiments, as seen below, are well suited for high quality measurement of jets and $\not\!\!E_T$ at the LHC.

2.1. CMS Calorimeters

The CMS electromagnetic calorimeters use lead tungstate crystals with a thickness of about 25 radiation lengths and cover the pseudorapidity up to $|\eta| < 3.0$. A very fine granularity is achieved with a typical cell size of $\Delta\eta \times \Delta\phi = 0.0174 \times 0.0174$. The readout of scintillation light is performed by silicon avalanche photodiodes in the barrel region and vacuum phototriodes in the endcap region. A preshower system is installed in front of the endcap electromagnetic calorimeters for π^0 rejection. Positioned outside the electromagnetic calorimeters are the brass/scintillator sampling hadron calorimeters

with a coarser granularity of $\Delta\eta \times \Delta\phi = 0.087 \times 0.087$ in the barrel and $\Delta\eta \times \Delta\phi =\sim 0.09\times \sim 0.17$ in the endcap regions. The barrel hadron calorimeter is complemented by a tail-catcher, ensuring that hadronic showers are sampled with nearly 11 hadronic interaction lengths. Coverage up to a pseudorapidity of 5.0 is provided by iron/quartz-fiber forward calorimeters.

2.2. ATLAS Calorimeters

The ATLAS electromagnetic calorimeters covering the pseudorapidity range of $|\eta| < 3.2$ have liquid argon/lead accordion structure. The hadronic calorimeters surrounding them are scintillating tile/iron in the central region ($|\eta| < 1.7$) and parallel plate liquid argon/copper in the endcap region ($1.7 < |\eta| < 3.2$). The forward region is covered by liquid argon/copper or tungsten calorimeter with a tubular electrode readout accommodating the high ionization rates expected at LHC at design luminosity. The readout of the calorimeters is highly granular for the electromagnetic compartments with typically three longitudinal samplings with varying lateral cell sizes, e.g. $0.0025 < \Delta\eta < 0.05$ and $0.025 < \Delta\phi < 0.1$ in the second segment containing the electromagnetic shower maximum. The hadronic calorimeters are coarser, with typically $\Delta\eta \times \Delta\phi = 0.1 \times 0.1$, but have also at least three longitudinal segments. The total number of readout cells in the ATLAS calorimeter system is about 200,000. The total thickness of the ATLAS calorimeter system for hadrons is at least 10 absorption lengths over the whole acceptance region.

3. JET RECONSTRUCTION AND CALIBRATION

3.1. Jets in ATLAS

Jet finder implementations most commonly used in ATLAS are a seeded fixed cone algorithm with split and merge [4], and sequential recombination algorithms like a k_T, anti-k_T and Cambridge/Aachen [5]. The seeded cone algorithm, where a jet is formed from signal objects within a $\eta - \phi$ cone of radius $R_{\rm cone}$ around the seed above certain thresholds. This algorithm is not infrared safe, which can be partly recovered by introducing a split and merge step after the jet formation. The seed threshold is usually chosen to be $p_T > 1$ GeV, and a narrow ($R_{\rm cone} = 0.4$) and a wide cone jet ($R_{\rm cone} = 0.7$) options are used. The sequential recombination algorithms are more robust and better motivated from the infrared and collinear safety. ATLAS has examined experimental aspects of the algorithms such as jet reconstruction efficiency and response linearity as well as the sensitivity to noise and pile-up, etc, and decided to concentrate calibration efforts on anti-k_T algorithm for early data analysis.

Several calibration approaches are currently present in ATLAS, based on the calorimeter response on the cell level or layer level and either in the context of jets or of clusters [6]. Most commonly used so far is a global calibration where the calorimeter jet is corrected to the particle jet using cell weights obtained by minimizing the jet energy resolution with respect to the particle jet. The performance of the calibration in terms of jet linearity and resolution has been assessed in a variety of physics processes like QCD dijets, top-pairs and SUSY events. Alternative global calibration method utilizes the energy deposits in the longitudinal calorimeter samplings to correct for calorimeter non-compensation. This method is simple and less demanding in terms of agreement between the detector simulation predictions and real data. Both global calibration techniques can be complemented by in-situ calibrations using physics processes. Figure 1 shows the jet energy response and resolution for jets reconstructed at the electromagnetic scale and for jets calibrated with the two global calibration methods.

Another calibration approach is a local hadron calibration, where the calorimeter clusters are reconstructed and calibrated to the hadronic scale *before* the jet is formed [6]. In this calibration scheme the clusters are reconstructed with a noise suppression and then classified as hadronic or electromagnetic clusters based on shower shapes and other cluster characteristics. The hadronic clusters are subject to a cell weighting procedure to compensate for calorimeter response and energy deposits in dead material as simulated by single pion Monte Carlo simulations. Additional energy scale correction is needed to restore the

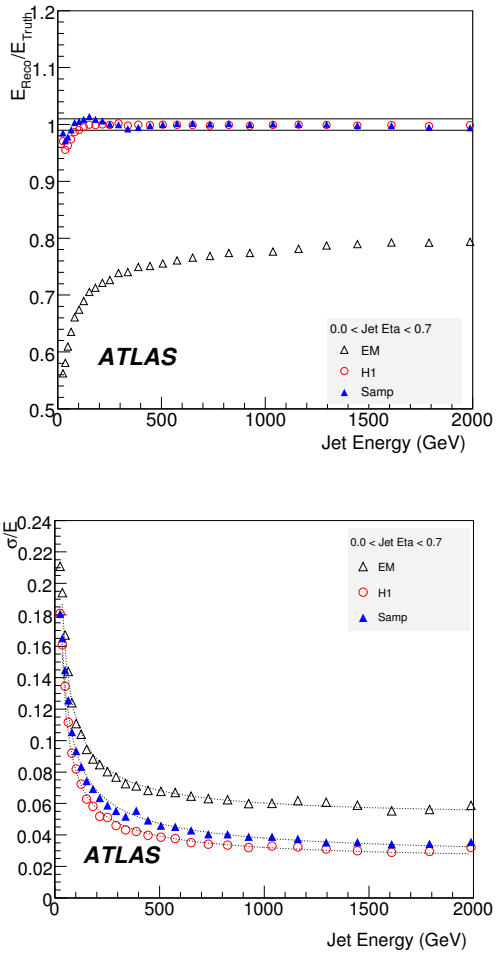

Figure 1. Jet energy response (top) and resolution (bottom) in the pseudorapidity region $|\eta| < 0.7$ as a function of jet energy. The open triangle points are for jets reconstructed at the electromagnetic scale (EM). The open circle and closed triangle points are for jets calibrated with global calibration scheme based on cell energy density and calorimeter layers, respectively.

particle level jet energy.

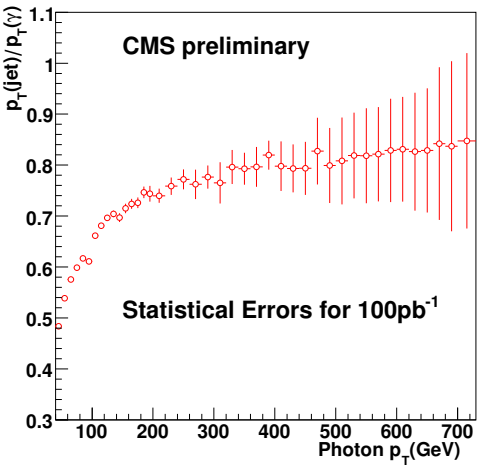

Figure 2. Transverse momentum ratio of the jet to the photon as a function of the photon p_T in γ + jet events, expected in 100 pb^{-1} of integrated luminosity.

3.2. Jet in CMS

CMS also plans to support and calibrate a number of jet clustering algorithms with various input objects. Mainly used in CMS are anti-k_T, k_T and seedless infrared safe cone algorithm, which is infrared safe to all orders in perturbative expansion and does not apply any p_T threshold to the input objects. As for jet inputs, options are calorimeter towers and particles reconstructed with the "particle-flow" algorithm, which is described in a separate section. Calorimeter jets can be optionally corrected using the measured momentum of charged particle tracks, providing "Jet-PlusTracks" (JPT) physics objects.

Global jet calibration at CMS is based on a factorized multi-level jet correction [7], in which many of the corrections can be obtained from in-situ collision data, and applied to either calorimeter, JPT and particle-flow jets in the following sequence; offset, relative η, and absolute p_T corrections. Figure 2 shows an example of absolute p_T correction using p_T balance between the pho-

ton and jet in γ + jet events. Optional corrections for jet electromagnetic energy fraction, jet flavor, underlying events and out-of-cone energy (for parton-level correction) can be used in this sequence after the absolute correction. For early LHC running, the plan is to use corrections derived from Monte Carlo truth information until the data-driven calibration analysis is completed.

4. MISSING E_T RECONSTRUCTION AND CALIBRATION

The missing transverse energy is primarily reconstructed from energy deposits in the calorimeter at both ATLAS and CMS experiments. Apart from the hard scattering process of interest, many other sources such as underlying events, multiple interactions, pile-up and coherent electronics noise, lead to energy deposits. Muons will deposit only a small energy in the calorimeters. Classifying the energy deposits into various physics objects and calibrating them accordingly is the essential key for an optimal $\not\!\!E_T$ measurement. In addition, the loss of energy in dead regions and readout channels make the $\not\!\!E_T$ measurement a real challenge.

4.1. Missing E_T in ATLAS

In ATLAS the standard $\not\!\!E_T$ is reconstructed from the energy deposits in calorimeter cells which survive a noise suppression procedure [6]. By default the noise suppression is performed on 3-dimensional topological calorimeter clusters, where the absolute energy in a seed (neighbor, boundary) cell is required to be larger than 4 (2, 0) times σ_{noise}, the width of the noise distribution due to pure electronics noise and/or the combination of electronics and pile-up noise. Calibration to cell energies is done using global cell-level weights depending on the energy density (referred to as global calibration) and/or calibration weights for the reconstructed physics object that the cell is assigned to (referred to as refined calibration). Corrections for muon(s) in events and the energy loss in dead materials are applied. Shown in Fig. 3 are the performance of $\not\!\!E_T$ response linearity and resolution with global and/or refined calibrations for different physics processes.

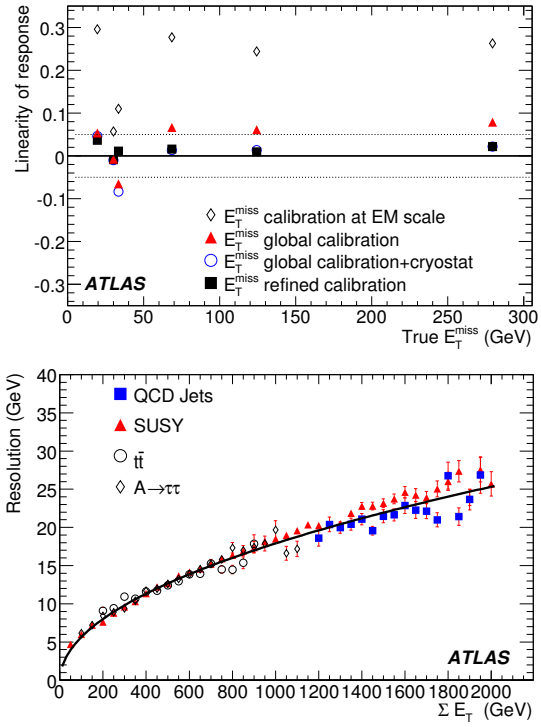

Figure 3. (Top) Missing E_T response linearity as a function of the average true $\not\!\!E_T$ for six different physics processes (from left to right: $Z \to \tau\tau$, $W \to e\nu$, $W \to \mu\nu$, semi-leptonic $t\bar{t}$, SUSY Higgs $A \to \tau\tau$ of $m_A = 800$ GeV, and SUSY with the mass scale of 1 TeV). Different points correspond to different $\not\!\!E_T$ calibration steps, and the filled square points are for refined $\not\!\!E_T$. (Bottom) Resolution of the two $\not\!\!E_T$ components with refined calibration as a function of the scaler transverse energy $\sum E_T$. The curve represents a best fit of $\sigma = 0.57\sqrt{\sum E_T}$ through the points from $A \to \tau\tau$ events.

4.2. Missing E_T in CMS

At CMS the $\not\!\!E_T$ is reconstructed from the transverse vector sum over all uncorrected energy deposits in projective calorimeter towers [8]. The $\not\!\!E_T$ performance is investigated using Monte Carlo simulation of QCD dijet events with $20 < \hat{p}_T < 800$ GeV, as shown in Fig. 4 where the resolution σ of the $\not\!\!E_T$ is plotted as a function of the event scaler transverse energy ($\sum E_T$). A fit to the resolution with the form of

$$\sigma = A \oplus B\sqrt{\sum E_T - D} \oplus C(\sum E_T - D) \quad (1)$$

yields the stochastic term B to be 103 % and the constant term C to be 2.3 %. The slightly higher stochastic term than the physics TDR result of 97 % is attributed to the calorimeter simulation significantly improved to reflect more realistic detector performance.

The basic calorimeter-based $\not\!\!E_T$ measurement can be improved by correcting $\not\!\!E_T$ for the jet energy scale, muons, isolated τ-jets, and unclustered energy deposits due to soft underlying events and pile-up. Figure 4 shows the effect of the jet response correction in $W(\rightarrow e\nu)$ + jets Monte Carlo samples. Shown in the figure is the bias (i.e, measured minus true $\not\!\!E_T$) projected onto the direction of the neutrino from the W-boson decay as a function of the true $\not\!\!E_T$. The Monte Carlo-based jet corrections remove the bias almost entirely over the wide range of $\not\!\!E_T$. CMS has options to calculate $\not\!\!E_T$ from tracks as well as particles using particle-flow algorithm, described in the next section.

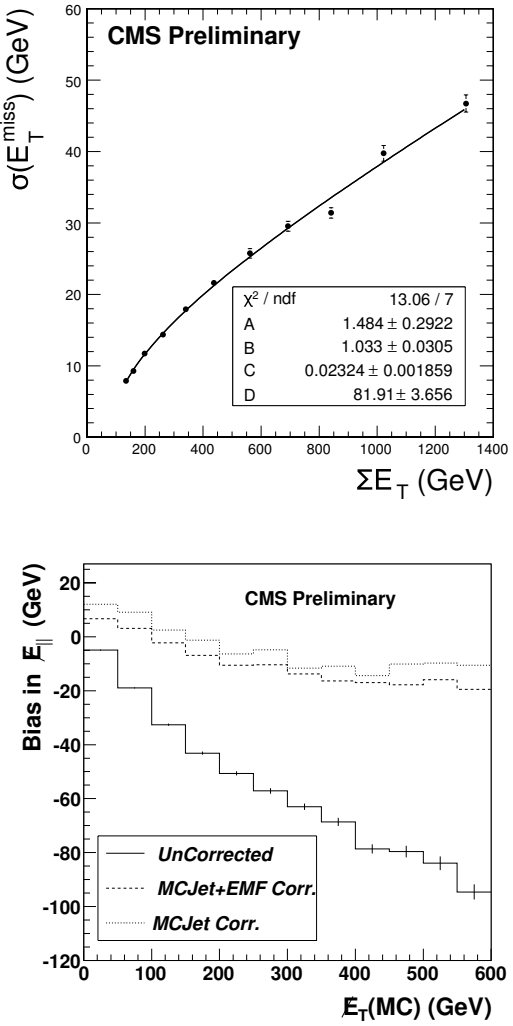

Figure 4. (Top) Missing E_T resolution for QCD dijet events with $20 < \hat{p}_T < 800$ GeV. The curve shows a fit to the resolution with a functional form and fit parameters given in Eq.(1). (Bottom) Missing E_T bias along the direction of the neutrino from W decay in $W(\rightarrow e\nu)$ + jets events. The three histograms correspond to different correction steps: raw (solid), MC-based jet correction only (dotted), and MC-based correction plus electromagnetic fraction correction for jets (dashed).

5. Particle-Flow Reconstruction in CMS

The particle-flow (PF) event reconstruction in CMS [9] aims to reconstruct and identify as many stable particles in the final state, i.e, electrons, muons, photons, charged and neutral hadrons, as possible by exploiting a full combination of all CMS sub-detectors. Jets and $\not\!\!E_T$ are reconstructed by applying the standard algorithms (previously mentioned) to the list of identified particles in the events. The particle-flow technique starts with reconstructing fundamental *elements* such as charged tracks, calorimeter clusters and muon tracks, that are fed into the linking al-

gorithm where the elements are linked together to form single particles. To achieve a high efficiency detection of low p_T particles in jets and a separation of close energy deposits, advanced tracking and clustering algorithms have been developed for the element reconstruction. At the linking stage each pair of elements in the event is examined in terms of the distance between the elements, and the *blocks* of elements linked directly or indirectly are created. The blocks of elements are then used as inputs to the particle reconstruction and identification algorithms. The PF identification algorithm produces the"PF muons" from global muon reconstruction of the inner and muon tracking detectors, and then PF electrons from ECAL cluster deposits associated with the tracks. After each identification step the tracks and/or calorimeter clusters associated with the identified physics objects are removed from the block and not used in later processing. After the electron identification, HCAL cluster signals with tracks are used to determine the presence of PF charged hadrons. Comparing the calibrated cluster energies with the total track momentum, if the excess energy is found in the cluster energy, the excess is used to form PF photons and PF neutral hadrons depending on the amount of excess energy and the ECAL energy.

The PF reconstruction performance on jets and $\not\!\!E_T$ is examined with physics events by comparing the response and resolution between in the calorimeter-only reconstruction (with or without MC-based corrections mentioned above) and in the PF reconstruction. Shown in Fig. 5 is the jet response for jets with $40 < p_T < 60$ GeV and $|\eta| < 1.5$ and relative jet energy resolution as a function of jet p_T at $|\eta| < 1.5$. Note that the calorimeter-only jets are corrected by the previously mentioned MC-based jet energy scale corrections in the resolution plot, but not in the response plot. Figure 6 shows the $\not\!\!E_T$ response and resolution for the two reconstruction algorithms in semi-leptonic $t\bar{t}$ events. The calorimeter-only $\not\!\!E_T$ is corrected for jet energy scale and muons in the event. The PF $\not\!\!E_T$ scale linearity turns out to hold within ± 5 % at $\not\!\!E_T > 20$ GeV. As seen in the figure, a significant improvement (up to a factor of 2) is foreseen with the PF algorithm in relative $\not\!\!E_T$ resolution.

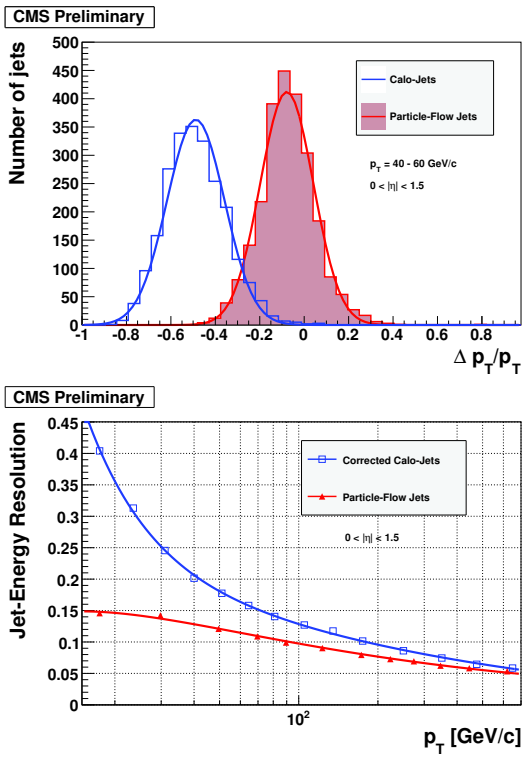

Figure 5. (Top) Jet response for calorimeter-only jets (open histogram) and particle flow jets (filled histogram), defined as the ratio $(p_T^{rec} - p_T^{gen})/p_T^{gen}$, for $40 < p_T^{gen} < 60$ GeV and $|\eta| < 1.5$ where "gen" and "rec" stand for generated and reconstructed jets, respectively. (Bottom) Jet energy resolution as a function of jet p_T for corrected calorimeter jets (open points) and particle flow jets (filled points).

6. HIGH p_T JET SIGNATURE

Search for new physics beyond the standard model using dijet signature is actively pursued by both collaborations. One of the QCD measurements that are sensitive to new physics is an inclusive p_T spectrum of the jets. Figure 7 shows

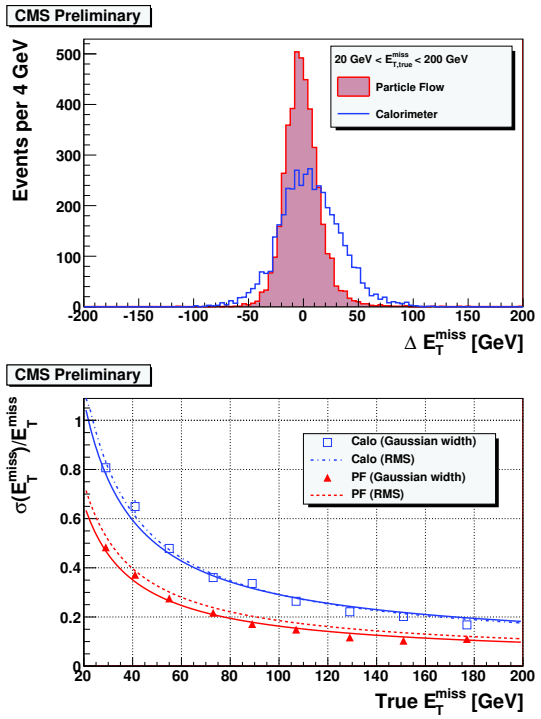

Figure 6. (Top) Missing E_T response for calorimeter-only $\not\!\!E_T$ (open histogram) and particle flow $\not\!\!E_T$ (filled histogram), defined as $\not\!\!E_T{}^{reco}$ - $\not\!\!E_T{}^{gen}$ for $\not\!\!E_T{}^{gen}$ = 20-200 GeV in semi-leptonic $t\bar{t}$ events. (Bottom) Missing E_T resolution as a function of true $\not\!\!E_T$ for calorimeter-only $\not\!\!E_T$ (open points) and particle flow $\not\!\!E_T$ (filled points). The solid (dashed) curve represents a fit to the resolution obtained from the sigma of the Gaussian fits to each $\not\!\!E_T$ bin (RMS of the $\not\!\!E_T$ bin).

the generator level distribution of jet yield in the pseudorapidity range $|\eta| < 1$ for an integrated luminosity of 10 pb^{-1} at the center of mass energy 14 TeV [10]. Superimposed are the expectations for the presence of contact interactions with scale of 3 and 5 TeV. It is clearly seen that the discovery of contact interactions is possible in early LHC running of $\sim$ 10 pb^{-1} data, where the error at high p_T will be dominated by jet energy scale uncertainty ($\sim$ 10 % shown as a shaded band). The figure also shows the fractional difference from the QCD distribution due to contact interaction signals and statistical and systematic uncertainties. CMS concludes that a contact interaction can be discovered beyond the current Tevatron exclusion of $\Lambda^+ < 2.7$ TeV with 10 pb^{-1} of data.

Measurement of dijet mass spectrum can also be a powerful probe to new physics making a dijet resonance signature. The QCD background can be estimated using a fit to the spectrum or Monte Carlo simulation predictions. Figure 8 shows the dijet mass spectra at the generator level, calorimeter level and the calorimeter level corrected for calorimeter non-uniformity and response. Expected deviations due to the presence of excited quark signals (with mass of 0.7, 2 and 5 TeV) from QCD spectrum indicate that we will have a strong discovery potential for a 2 TeV excited quark with 100 pb^{-1} of data [10].

Recently a great interest has grown on new physics search with an exotic signature of highly boosted heavy objects decaying to quarks. A typical example is a high p_T top-quark production from a massive resonance decaying to a $t\bar{t}$. In a scenario of warped extra dimensions proposed by Randall and Sundrum [11], where all the standard model fields propagate in the bulk of extra dimensions [12], a Kaluza-Klein (KK) excitation of the gluon $g^{(1)}$ with a $\sim$TeV mass scale strongly couples to quarks and decays to a $t\bar{t}$-pair with a very large branching fraction ($\sim$ 93 %). The cross section of the KK gluon production at the LHC ($\sqrt{s}$ = 14 TeV) is about 30 (0.4) pb for the $g^{(1)}$ mass of 1 (3) TeV. Top quarks from the decay of massive KK gluons are thus highly boosted, and the decay products of the top quark often merge into a single jet (i.e, a top *mono*-jet). Reconstruction and identification of such top mono-jet signatures impose a new challenge as the standard algorithm can no longer distinguish the decay products. Shown in Fig. 9 is the effect of the merging. Seeded cone jets with a radius $R_{\rm cone} = 0.4$ are reconstructed in the vicinity of the top quarks, and the fraction of the time the W-boson and b-quark from the top decay fall within a distance $R = 0.4$ of the jet direction is measured. A top mono-jet is defined in the figure as the jet containing both

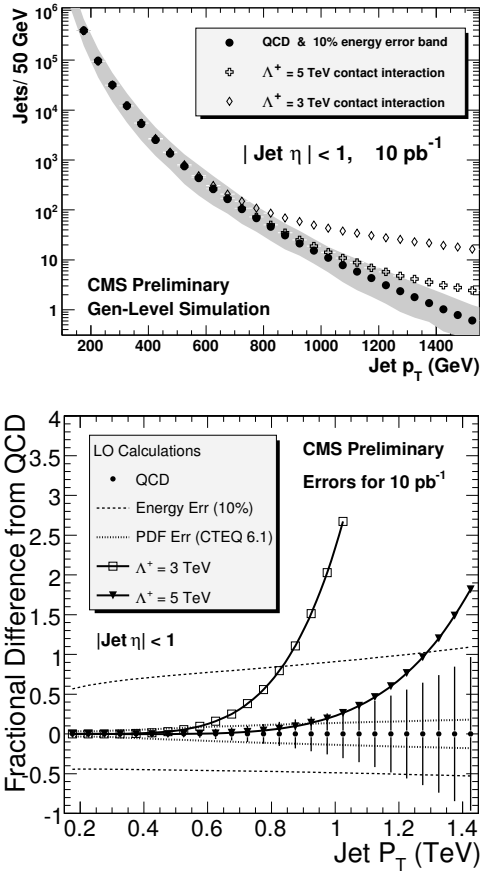

Figure 7. (Top) Number of generated jets ($|\eta| < 1$) expected from QCD in 50 GeV bins for an integrated luminosity of 10 pb^{-1}. The QCD distribution (filled points) is modified by the presence of contact interactions with scale $\Lambda^+ = 3$ TeV and 5 TeV (open points). The shaded band corresponds to a 10 % uncertainty on jet energy scale. (Bottom) Fractional difference from QCD prediction in inclusive jet p_T spectrum due to various systematic sources and the presence of contact interactions with scale $\Lambda^+ = 3$ TeV and 5 TeV. for an integrated luminosity of 10 pb^{-1}. The errors on the points are the statistical uncertainties in the QCD prediction and the dashed (dotted) curve represents the uncertainty due to jet energy scale (PDF).

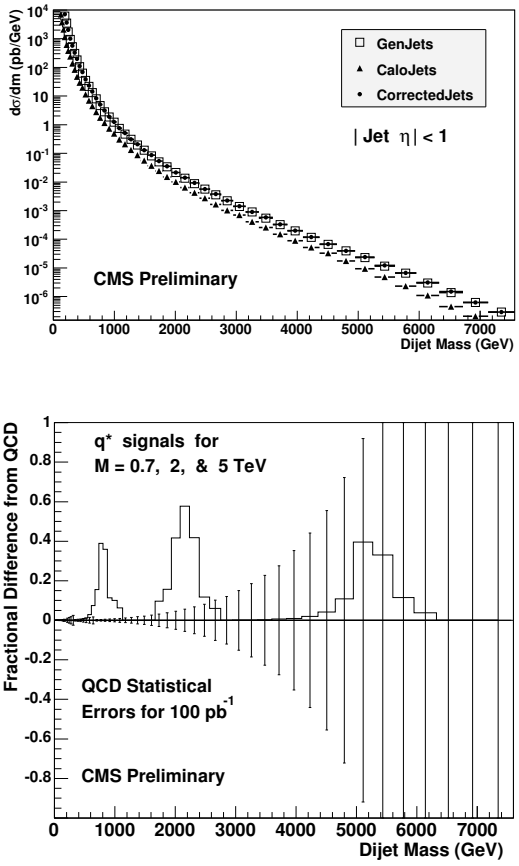

Figure 8. (Top) Dijet mass differential cross section expected from QCD for $|\eta| < 1$ from generated jets (squares), calorimeter jets (triangles) and corrected calorimeter jets (circles). (Bottom) Fractional difference between the QCD and excited quark ($q*$) signals of mass 0.7, 2 and 5 TeV in dijet mass spectrum obtained from corrected calorimeter jets for an integrated luminosity of 100 pb^{-1}.

the W-boson and the b-quark. As expected, the probability of the merging steadily rises with the p_T of the top quark, and it is reconstructed as a single jet at almost 80 % of the time if the top p_T

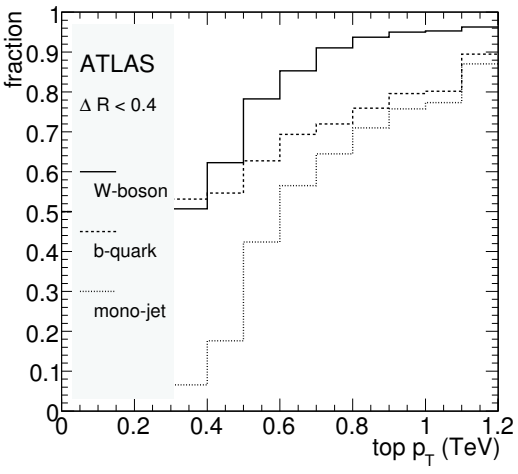

Figure 9. Fraction of the top quark decays, where a W-boson (solid line) or a b-quark (dashed line) falls into a cone of radius $R = \sqrt{\Delta\eta^2 + \Delta\phi^2}$=0.4 drawn around the jet reconstructed in the top quark direction, as a function of the p_T of the top quark. The mono-jet case (dotted line) shows the fraction of both W-boson and b-quark falling within the cone.

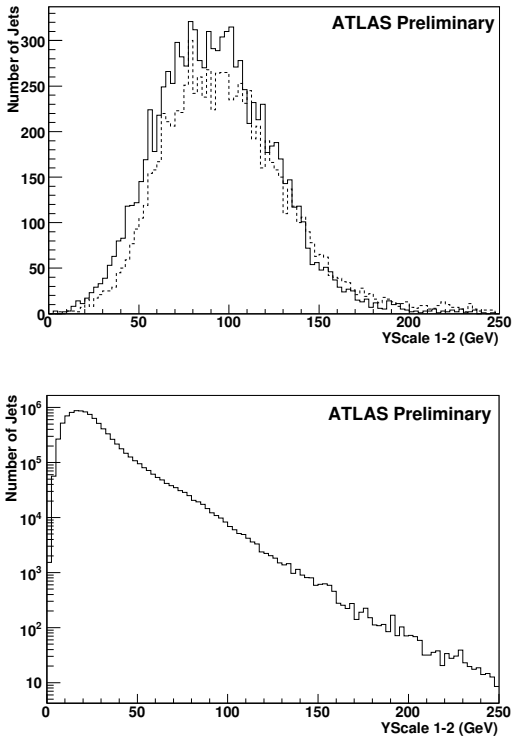

Figure 10. k_T distance scale corresponding to the top mono-jets splitting into two jets for (top) the $Z' \to t\bar{t}$ of mass 2 (solid) and 3 (dashed) TeV, and (bottom) QCD background. For the Z' signal the events are selected in which only a single jet with $p_T > 300$ GeV has the η-ϕ distance of $\Delta R < 1.0$ from the closest top quark and $\Delta R < 2.0$ from the hadronically decaying W-boson.

exceeds 1 TeV.

ATLAS approach for the identification of merged top mono-jets is based on the mass and sub-structure of the jet [13] and the lifetime signature for b-quark. The top mono-jets (composed of three quark jets for the hadronic W decay) reconstructed with k_T algorithm have the k_T distance scales corresponding to the splitting of the mono-jet into two, three, four, ... sub-jets. These k_T distance (splitting) scales are a good discriminator between the top jets and regular QCD jets; one of the scales at which a mono-jet is split into two jets is shown in Fig. 10 for standard model-like heavy Z'-boson ($\to t\bar{t}$) of the mass of 2 and 3 TeV. A mass of the top mono-jet (not shown), peaked around 170-200 GeV, is also a useful variable to enhance the top signal. A long lifetime of B-hadrons and the resulting large impact parameters of the B-hadron decay tracks are generally a good tool to tag the top events. Again the "b-tagging" poses a challenge for the high p_T top due to merging effects; degradation of track reconstruction efficiency and increasing mis-reconstructed tracks, poorer matching between the mono-jet and b-quark directions, etc.

7. SUMMARY

Reliable reconstruction and calibration of jets and missing transverse energy at the LHC are one of the most important ingredients to understand the standard model and have a glimpse of new physics signatures beyond that at the LHC. Development of robust and flexible reconstruction procedure suited for early LHC running and detailed understanding of the calibration steps for precise measurements are in progress in both ATLAS and CMS experiments. Monte Carlo-based calibrations have been extensively tested and proved to work well, providing a good reference for development of data-driven calibration techniques. The experiments aim to provide a robust estimate of jet and missing energy uncertainties with in-situ measurement of various physics processes.

A measurement of high transverse momentum jets in dijet events have the potential to discover new physics in early LHC data. A new physics could manifest itself in a more exotic signature of high p_T jets and an example is a boosted top quark with a mono-jet signature. Only a few examples are given for the identification algorithms for boosted top quarks, and many more studies are in a rapid progress in both collaborations.

REFERENCES

1. CMS Collaboration, The CMS experiment at the CERN LHC, JINST **3** S08004 (2008).
2. ATLAS Collaboration, Detector and Physics Performance Technical Design Report, CERN/LHCC/99-14/15 (1999).
3. CMS Collaboration, CMS Physics : Technical Design Report, CERN/LHCC/06-01 (2006).
4. G. C. Blazey et. al., Run II Jet Physics, hep-ex/0005012v2 (2000).
5. M. Cacciari, G. P. Salam, Phys. Lett. B **641**, 57 (2006).
6. ATLAS Collaboration, Expected Performance of the ATLAS Experiment - Detector, Trigger and Physics, CERN-OPEN-2008-020, arXiv:0901.0512v4 (2009).
7. CMS Collaboration, Plans for Jet Energy Corrections at CMS, CMS-PAS-JME-07-002 (2008).
8. CMS Collaboration, Missing E_T performance in CMS, CMS-PAS-JME-07-001 (2007).
9. CMS Collaboration, Particle-Flow Event Reconstruction in CMS and Performance for Jets, Taus, and E_T^{miss}. CMS-PAS-PFT-09-001 (2009).
10. CMS Collaboration, CMS Search Plans and Sensitivity to New Physics using Dijets, CMS-PAS-SBM-07-001 (2007).
11. L. Randall and R. Sundrum, Large Mass Hierarchy from a Small Extra Dimension, Phys. Rev. Lett. **83**, 3370 (1999).
12. B. Lillie, L. Randall and L. T. Wang, The Bulk RS KK-gluon at the LHC, JHEP **0709**, 074 (2007).
13. G. Brooijmans, High p_T Hadronic Top Quark Identification Part I : Jet Mass and YSplitter, ATL-PHYS-CONF-2008-008 (2008).